Evaluation of electron capture reaction rates in Ni isotopes in stellar environments

Toshio Suzuki,[1,2,3] Michio Honma,[4] Hélène Mao,[5] Takaharu Otsuka,[6,7] and Toshitaka Kajino[3,8]

[1]*Department of Physics and Graduate School of Integrated Basic Sciences, College of Humanities and Sciences, Nihon University Sakurajosui 3-25-40, Setagaya-ku, Tokyo 156-8550, Japan*

[2]*Center for Nuclear Study, University of Tokyo, Hirosawa, Wako-shi, Saitama 351-0198, Japan*

[3]*National Astronomical Observatory of Japan, Mitaka, Tokyo 181-8588, Japan*

[4]*Center for Mathematical Sciences, University of Aizu, Aizu-Wakamatsu, Fukushima 965-8580, Japan*

[5]*ENSPS, Pôle API–Parc d'Innovation, Boulevard Sébastien Brant, BP 10413, F-67412 Illkirch Cedex, France*

[6]*Department of Physics and Center for Nuclear Study, University of Tokyo, Hongo, Bunkyo-ku, Tokyo 113-0033, Japan*

[7]*National Superconducting Cyclotron Laboratory, Michigan State University, East Lansing, Michigan 48824, USA*

[8]*Deaprtment of Astronomy, Graduate School of Science, University of Tokyo, Bunkyo-ku, Tokyo 113-0033, Japan*

(Received 10 November 2010; revised manuscript received 28 February 2011; published 27 April 2011)

Electron capture rates in Ni isotopes are studied in stellar environments, that is, at high densities and high temperatures during the core-collapse and postbounce explosive nucleosynthesis in supernovae. Reaction rates in ^{58}Ni and ^{60}Ni, as well as in ^{56}Ni, ^{62}Ni, and ^{64}Ni, are evaluated by shell-model calculations with the use of a new shell-model Hamiltonian in the fp shell, GXPF1J. While the previous shell-model calculations failed to reproduce the measured peaks of Gamow-Teller strength in ^{58}Ni and ^{60}Ni, the present new Hamiltonian is found to reproduce them very well, as well as the capture rates obtained from the observed strengths. Strengths and energies of the Gamow-Teller transitions in ^{56}Ni, ^{62}Ni, and ^{64}Ni are also found to be consistent with the observations.

DOI: 10.1103/PhysRevC.83.044619 PACS number(s): 23.40.−s, 21.60.Cs, 25.40.Kv, 27.40.+z

I. INTRODUCTION

Electron capture reactions play a critical role in determining the electron-to-baryon ratio Y_e, namely, the fraction of protons in the protoneutron star, and also the core entropy at the final stage of collapsing supernovae. Frequent electron captures act to reduce leptonic pressure and also accelerate generation of neutrinos which carry away both internal energy and entropy from the core. Electron captures are suggested to eventually affect the size of the emergent homologous core and even the iron core. Y_e is also one of the important initial conditions for incomplete silicon burning during postbounce explosive nucleosynthesis. The abundance of elements produced in supernovae is sensitive to the value of Y_e. It is, therefore, important to evaluate the electron capture rates at high densities and high temperatures very accurately.

Electron capture reactions were studied in Ref. [1] (hereafter referred to as FFN), and capture rates were obtained based on a simple shell model as well as using available experimental Gamow-Teller (GT) strengths. Evaluations of the reaction rates have been improved by large-scale shell-model calculations [2]. The method by FFN overestimates the capture rates of the shell-model calculations in many cases [2–4]. Capture rates in fp-shell nuclei are obtained by shell-model calculations with the use of KB3 Hamiltonians [5], and they are tabulated for a wide range of nuclei [4].

Using a $(d, {}^2\mathrm{He})$ reaction, GT_+ strength [see Eq. (1)] distribution in ^{58}Ni was measured, and electron capture rates obtained from the measured GT_+ strength were compared with the rates obtained by large-scale shell-model (LSSM) calculations [6]. The calculated rates obtained by using the KB3G Hamiltonian [7] were found to be improved as compared with those obtained by the KBF Hamiltonian [8]. The GT_+ strength in ^{60}Ni was also measured by a (n, p) reaction and the electron capture rates obtained from the observed GT_+ strengths were compared with those by LSSM calculations with the use of the KBF [9]. As this interaction fails to produce the observed peak of the GT_+ strength at $E_x = 0.65$ MeV, the capture rates of the LSSM calculations underestimate the experimental values significantly at lower temperature.

Here, we use a new shell-model Hamiltonian for the fp shell, GXPF1J [10], in order to improve this defect, and newly evaluate the capture rates by shell-model calculations. The KB3G, the most recent version of the KB3's, is also used.

In the next section, we explain how the new Hamiltonian GXPF1J was constructed. The GXPF1J is shown to reproduce well the magnetic dipole (M1) and GT transitions in fp-shell nuclei. In Sec. III, electron capture reaction rates in Ni isotopes are evaluated by shell-model calculations with the use of GXPF1J at high densities and temperatures. A summary is given in Sec. IV.

II. NEW HAMILTONIAN GXPF1J

The GXPF1J Hamiltonian was defined by applying two modifications to the original GXPF1 Hamiltonian [11]. The GXPF1 was obtained by fitting to 699 experimental energy data of fp-shell nuclei in a wide range of mass numbers, $A =$ 47–66. The ^{56}Ni nucleus is found to be a soft core with 69% $(0f_{7/2})^{16}$ configurations. Energy levels of the 2_1^+ states and $B(E2; 0^+_{\mathrm{g.s.}} \to 2^+_1)$ values of fp-shell nuclei are systematically well explained by GXPF1. The Hamiltonian is also successful in describing the spin-dependent transitions in fp-shell nuclei.

TABLE I. Calculated energy of the peak position of the M1 strength and the B(M1) value in ^{48}Ca. The fraction of the strength of the 1^+ state is denoted in the parentheses. Experimental values [13] are also given.

Hamiltonian	E_x (MeV)	B(M1) (μ_N^2) (ratio to total strength)
GXPF1	10.95	9.5 (88%)
GXPF1A	10.90	9.0 (83%)
GXPF1J	10.22	10.1 (93%)
KBF	9.27	7.3 (83%)
KB3G	9.21 and 9.37	4.3 (48%) and 4.3 (48%)
EXP. [13]	10.23	3.9 ± 0.3 (74 ± 14%)

The first modification was made to improve the description of new experimental data of neutron-rich Ca, Ti, and Cr isotopes with $N > 32$, which were not included in the fit. We modified five two-body matrix elements with isospin 1: The monopole pairing strength was made less attractive for the $f_{7/2}$-$f_{7/2}$, $f_{5/2}$-$p_{1/2}$, and $p_{1/2}$-$p_{1/2}$ orbits, and the quadrupole-quadrupole interaction was made more attractive for the $f_{5/2}$-$p_{1/2}$ orbits. The resultant Hamiltonian was GXPF1A [12]. The second modification, which defines GXPF1J [10], was adopted in order to reproduce the peak position of the M1 strength in ^{48}Ca. Experimentally, most of the M1 strength is concentrated on one state at 10.23 MeV [13], while GXPF1A predicts such a state at 10.90 MeV. We multiplied the *multipole* part of the diagonal two-body matrix elements with isospin 1 for the $f_{7/2}$-$f_{5/2}$ orbits by a common factor 0.7. Calculated energies and B(M1) strengths of the 1^+ state which exhausts most of the total M1 strength in ^{48}Ca are shown in Table I for various Hamiltonians. The experimental B(M1) strength $3.9 \pm 0.3\mu_N^2$, which exhausts 74 ± 14% of the total strength $5.3 \pm 0.6\mu_N^2$ [13], is reproduced with the quenching of the spin g factor, $g_s^{\rm eff}/g_s = 0.62 \pm 0.02$ for GXPF1J. The KBF and KB3G give energies for the 1^+ state $\sim$1 MeV below the experimental one. The M1 strength is split into two states in the case of KB3G.

The M1 transition strengths in ^{50}Ti, ^{52}Cr, and ^{54}Fe are reproduced for GXPF1J with the quenching of the spin g factor, $g_s^{\rm eff}/g_s = 0.75 \pm 0.02$ [14]. The Gamow-Teller (GT$_-$) transition strength in ^{58}Ni (^{58}Ni $\rightarrow$ ^{58}Cu) is also found to be well reproduced with the use of the quenching of the axial-vector coupling constant, $f_q = g_A^{\rm eff}/g_A = 0.74$ [5,15], as shown in Fig. 5 of Ref. [10]. Here,

$$B(\mathrm{GT}_\pm) = \frac{1}{2J_i+1}|\langle f\|\sum_k f_q\sigma_k t_{k\pm}\|i\rangle|^2, \qquad (1)$$

where $t_+|p\rangle = |n\rangle, t_-|n\rangle = |p\rangle$, and f_q is the quenching factor, which will be taken to be 0.74 hereafter.

Total GT$_+$ strengths and centroid energies of the GT$_+$ strengths obtained by various Hamiltonians are shown in Table II for Ni isotopes. Total GT$_+$ strengths are more or less similar for various Hamiltonians and rather close to the experimental values. On the other hand, the centroid energies are higher for GXPF1's compared to KB's, which means that the strengths are generally more fragmented and have more components in higher excitation energies in the case of GXPF1's. This feature is clearly seen for ^{56}Ni, ^{58}Ni, and ^{60}Ni in Sec. III. We will use GXPF1J for the evaluation of the electron capture rates in Sec. III. The KB3G is also used for comparison.

III. ELECTRON CAPTURE REACTION RATES IN NI ISOTOPES

A. ^{58}Ni and ^{60}Ni

Shell-model calculations are carried out by using the code MSHELL [16], allowing at most five nucleons to be excited from the $0f_{7/2}$ orbit into the upper orbits. The GT strength distributions are obtained by following the prescription of Ref. [17]. Calculated GT$_+$ strengths in ^{58}Ni and ^{60}Ni by GXPF1J are shown in Figs. 1 and 2, respectively. The summed values of B(GT$_+$) up to excitation energies of the daughter nuclei at E_x are also shown. Experimental GT$_+$ strengths are available both for ^{58}Ni [6] and ^{60}Ni [9]. The observed summed B(GT$_+$) values are also given in these figures.

The strengths for GXPF1J are found to be more fragmented with remaining tails at $E_x > 6$ MeV as compared to those for KB3G. In ^{58}Ni, a large peak of the strength is observed at $E_x = 1.868$ MeV [6]. The position of the peak is reproduced by KB3G, but the magnitude of the strength is larger by about twice [see Fig. 1(b)]. The experimental summed B(GT$_+$) values at $E_x \leqslant 4$ MeV are rather well described by GXPF1J, as shown in Fig. 1(b). In ^{60}Ni, both the position and the magnitude of the first peak of the experimental GT$_+$ strength at $E_x =$ 0.65 MeV are well reproduced by GXPF1J (see Fig. 2). The KB3G predicts the first peak with larger strength at a higher

TABLE II. Total GT$_+$ strengths [denoted as ΣB(GT$_+$)] and centroid energies of the strengths (denoted as $\bar{E}_x$) for ^{56,58,60,62,64}Ni obtained by various Hamiltonians, GXPF1's and KB's, with the universal quenching factor $f_q = 0.74$. Experimental total strength values are taken from Ref. [19].

Nucleus	ΣB(GT$_+$) ($\bar{E}_x$)					
	GXPF1	GXPF1A	GXPF1J	KBF	KB3G	EXP.
^{56}Ni	6.2 (5.2)	6.2 (5.2)	6.2 (5.0)	5.3 (4.4)	5.4 (3.7)	
^{58}Ni	4.7 (4.2)	4.7 (4.3)	4.7 (4.1)	4.2 (3.7)	4.0 (2.9)	3.8 ± 0.4
^{60}Ni	3.4 (3.0)	3.4 (3.1)	3.4 (2.8)	3.1 (2.7)	2.8 (2.4)	3.1 ± 0.1
^{62}Ni	2.0 (1.8)	1.9 (2.0)	1.9 (1.8)	2.0 (1.7)	2.0 (1.5)	2.5 ± 0.1
^{64}Ni	1.0 (0.8)	0.9 (0.9)	0.9 (0.8)	1.2 (0.5)	1.1 (0.5)	1.7 ± 0.2

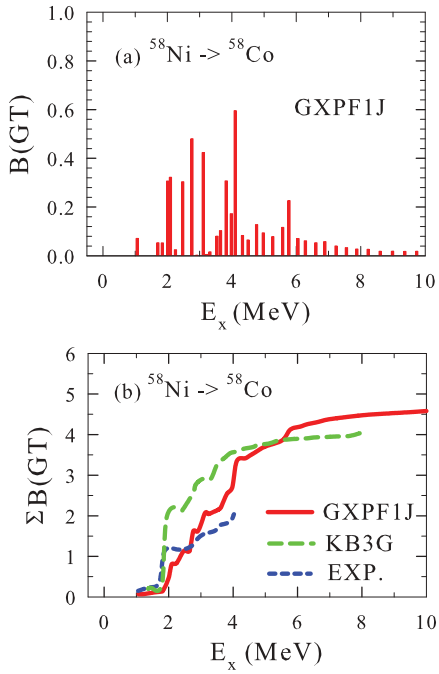

FIG. 1. (Color online) (a) GT strength for ^{58}Ni → ^{58}Co obtained by the shell-model calculation with the use of GXPF1J. (b) Sum of the GT strengths up to excitation energies of ^{58}Co, E_x, obtained for GXPF1J, KB3G, as well as the experimental data [6].

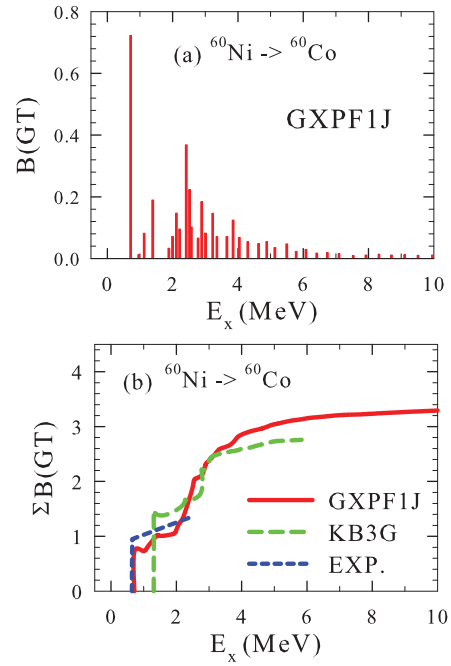

FIG. 2. (Color online) The same as in Fig. 1 for ^{60}Ni. The experimental B(GT) data are taken from Ref. [9].

excitation energy as compared to the observation. The strength at low energy, $E_x \leqslant 2$ MeV, is well described by GXPF1J.

Now, we evaluate the electron capture rates at high densities, $\rho Y_e = 10^7$–10^9 g/cm^3, and high temperatures, $T = T_9 \times 10^9$ K with $T_9 = 1$–10. The capture rates are calculated by

$$\begin{aligned}\lambda &= \frac{\ln 2}{6146(s)} \sum_i W_i \sum_f B(\mathrm{GT}; i \to f) \\ &\quad \times \int_{\omega_{\min}}^{\infty} \omega p (Q_{ij} + \omega)^2 F(Z, \omega) S_e(\omega) d\omega, \\ Q_{if} &= (M_p c^2 - M_d c^2 + E_i - E_f)/m_e c^2, \\ W_i &= (2J_i + 1) e^{-E_i/kT} / \sum_i (2J_i + 1) e^{-E_i/kT}, \end{aligned} \tag{2}$$

where ω and p are the electron energy and momentum in units of $m_e c^2$, M_p and M_d are the nuclear mass of parent and daughter nuclei, respectively, and E_i, E_f are excitation energies of the initial and final states. $F(Z, \omega)$ is the Fermi function, and $S_e(\omega)$ is the Fermi-Dirac distribution for electrons where the chemical potential μ_e is determined from the density ρY_e by

$$\rho Y_e = \frac{1}{\pi^2 N_A} \left(\frac{m_e c}{\hbar} \right)^3 \int_0^{\infty} (S_e - S_p) p^2 \, dp, \tag{3}$$

where N_A is the Avogadro number and S_p is the Fermi-Dirac distribution for positrons with the chemical potential $\mu_p = -\mu_e$. The values of the chemical potential for electrons are shown in Table III. It can become as large as 5–10 MeV at high densities $\rho Y_e = 10^9$–10^{10} g/cm^3. It slightly decreases as the temperature increases. The reaction rates become larger at higher densities because of the large chemical potential. On the contrary, when the chemical potential gets smaller than the threshold energy of the electron capture reaction, $-Q_{if}$ in Eq. (2), at low densities, the reaction rates vanish in the limit of zero temperature, $T \to 0$ K.

Since it is sometimes important to include GT transitions from thermally populated excited states [1,18] in stellar interiors, we include transitions from the excited states of the parent nucleus in addition to the ground state with the

TABLE III. Electron chemical potential μ_e (in units of MeV) at high densities, $\rho Y_e = 10^7$–10^{10} g/cm^3, and high temperatures, $T = T_9 \times 10^9$ K.

ρY_e (g/cm^3)	T_9									
	1	2	3	4	5	6	7	8	9	10
10^7	1.200	1.133	1.021	0.870	0.698	0.534	0.404	0.310	0.244	0.196
10^8	2.437	2.406	2.355	2.283	2.192	2.081	1.952	1.808	1.653	1.493
10^9	5.176	5.162	5.138	5.105	5.062	5.010	4.948	4.877	4.797	4.708
10^{10}	11.116	11.109	11.098	11.083	11.063	11.039	11.011	10.978	10.940	10.898

partition function W_i. When we consider transitions only from the ground state of the parent nucleus, the weight factor W_i is equal to 1.

When temperature becomes high and excitation energies of excited states of the parent nucleus are low, the nucleus can be thermally excited and the population of the excited states can be large. In such a case, the transitions from the excited states can give important contributions to the capture rates.

Calculated electron capture rates in ^{58}Ni and ^{60}Ni are shown in Fig. 3. Results calculated by GXPF1J and KB3G, which include only the contributions from the transitions from the ground states of the parent nuclei, are compared with those obtained from the experimental $B(\mathrm{GT}_+)$ values [6,9].

As the first excited states in ^{58}Ni and ^{60}Ni are 2^+ states above $E_x = 1$ MeV, the effects of the transitions from thermally excited 2_1^+ state are expected to be insignificant for the temperature considered here, $T = 10^9$–10^{10} K∼0.1–1 MeV. Contributions from the transitions from the 2_1^+ states are evaluated in order to see if this conjecture is correct. In the case of GXPF1J, calculated rates which further include contributions from the 2_1^+ states at $E_x = 1.4545$ and 1.3325 MeV for ^{58}Ni and ^{60}Ni, respectively, are also shown by dotted points.

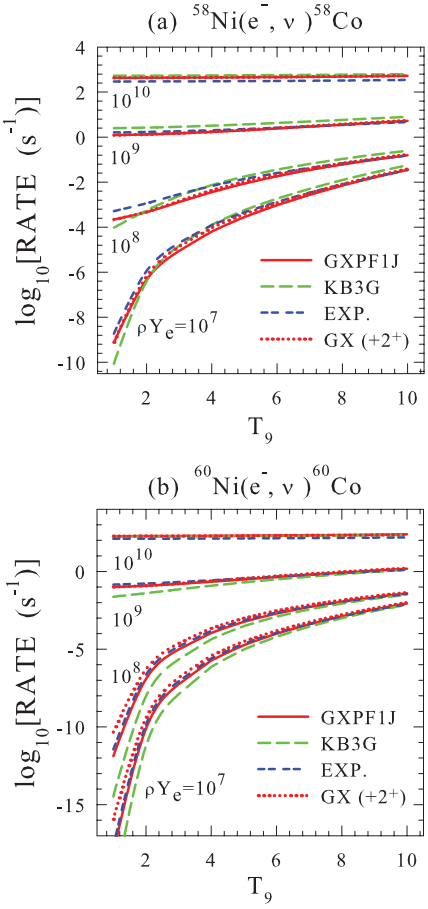

FIG. 3. (Color online) (a) Calculated electron capture rates on ^{58}Ni obtained by shell-model calculations with the use of GXPF1J (solid curves) and KB3G (dashed curves). The short-dashed curves are obtained by using the experimental $B(GT)$ values [6]. These curves include the contributions from the GT transitions from the ground state of ^{58}Ni only. Dotted points are obtained for GXPF1J by including the GT transitions from the 2_1^+ state of ^{58}Ni. (b) The same as in (a) for ^{60}Ni. The experimental B(GT) values of Ref. [9] are used.

In ^{58}Ni, the calculated capture rates for GXPF1J are suppressed as compared to those for KB3G except for $\rho Y_e = 10^7$–10^8 g/cm^3 at low temperatures. As the GT strength is more fragmented and has a remaining tail in the high-energy region for GXPF1J as we see from Fig. 1(b), it is more difficult to induce the capture reactions. In the case of $\rho Y_e = 10^7$–10^8 g/cm^3 at $T_9 \leqslant 2$, the GT transition to the 1_1^+ state at $E_x = 1.06$ MeV in ^{58}Co enhances the capture rates for GXPF1J, leading to larger rates than the case for KB3G. The lowest 1^+ state in ^{58}Co is observed at $E_x = 1.05$ MeV. In the case of KB3G, the 1_1^+ state is located at $E_x = 1.36$ MeV, in which case the electron chemical potential at $\rho Y_e = 10^7$ g/cm^3 is smaller than the value of $-Q_{if} = 2.35$ MeV ($E_i = 0.0$ MeV, $E_f = 1.36$ MeV, $M_d c^2 - M_p c^2 = 0.892$ MeV, and see Table III), and the rate decreases rapidly at low temperature and vanishes at $T = 0$ K.

We find that experimental capture rates are rather well reproduced by GXPF1J both in ^{58}Ni and ^{60}Ni. In particular, for ^{60}Ni, the agreement is excellent for GXPF1J. Note that the observed GT strength in ^{60}Ni is reproduced well by GXPF1J. Here, the first peak in the GT strength is important to obtain capture rates close to the experimental ones. In the case of KB3G, deviations from experimental capture rates in ^{60}Ni are within a factor of 3 at $T_9 > 3$–4.

The contributions from the excited 2_1^+ states to the capture rates are insignificant except for ^{60}Ni at $\rho Y_e = 10^7$ and 10^8 g/cm^3. This is due to a relatively large negative Q_{gg} value for ^{60}Ni ($Q_{gg} = -3.335$ MeV) as compared to the case for ^{58}Ni ($Q_{gg} = -0.892$ MeV). Here, $Q_{gg} = Q_{if} \times m_e c^2$ with $E_i = E_f = 0.0$ MeV in Eq. (2), that is, the initial and final states are ground states. As the transition from the ground state of ^{60}Ni is hard because of the large negative Q_{gg} value, the inclusion of the transition from the 2_1^+ state can affect the total transition strength and increase the capture rate.

In Ref. [4], capture rates are given for several limited cases of densities and temperatures. The cases for $\rho Y_e = 10^7$ g/cm^3 at $T_9 = 1$, 3, and 10 can be compared with the present results. The capture rates in the table are generally better than KB3G's. Note that experimental energies and strengths [19] are adopted in the table [4] when they are available.

We compare how much the capture rates can differ among the three GXPF1's. The calculated capture rates in ^{58}Ni and ^{60}Ni for GXPF1J, GXPF1, and GXPF1A are shown in Fig. 4. As there is no significant difference in the GT strengths, the differences of the capture rates are quite small except for the case of lower densities ($\rho Y_e = 10^7$–10^8 g/cm^3) and lower temperatures ($T_9 \leqslant 3$). In the case of ^{60}Ni, the GT strength for the first 1^+ state in ^{60}Co is smaller for GXPF1 and GXPF1A by 11% and 20%, respectively, as compared to that for GXPF1J. However, this difference hardly affects the capture rates because of the relatively large negative Q_{gg} value for the reaction on ^{60}Ni.

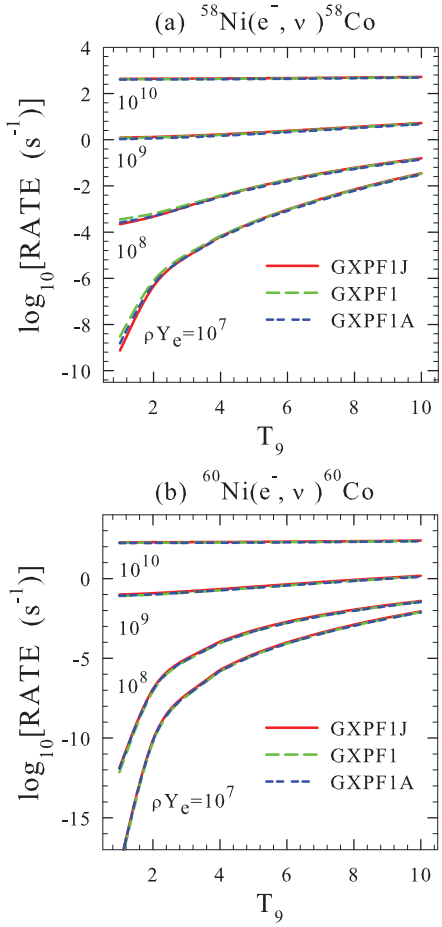

FIG. 4. (Color online) (a) Calculated electron capture rates on ^{58}Ni obtained by shell-model calculations with the use of GXPF1J (solid curves), GXPF1 (dashed curves), and GXPF1A (short-dashed curves). These curves include the contributions from the GT transitions from the ground state of ^{58}Ni only. (b) The same as in (a) for ^{60}Ni.

Hereafter, we use GXPF1J among the GXPF1's and also KB3G for comparison for the study of electron capture rates in other Ni isotopes, ^{56}Ni, ^{62}Ni, and ^{64}Ni.

B. ^{56}Ni

We discuss electron capture rates in ^{56}Ni. The nucleus ^{56}Ni is quite interesting as the GT strength distributions obtained by GXPF1J and KB3G differ considerably [see Fig. 2(a) of Ref. [20]]. In Ref. [20], this difference is shown to lead to the enhancement of the branching ratio for the proton emission channel, and the enhancement of the production yield of ^{55}Mn in population III stars through the neutrino-induced reactions, ^{56}Ni $(\nu, \nu' p)$ ^{55}Co (e^-, ν) ^{55}Fe (e^-, ν) ^{55}Mn. The summed values of the $B(\mathrm{GT}_+)$ obtained by GXPF1J and KB3G in ^{56}Ni up to excitation energy E_x of the daughter nucleus ^{56}Co are shown in Fig. 5(a). As we see from Fig. 5(a), there are two peaks in the GT distribution at $E_x \sim 3$ and 5 MeV for GXPF1J, while there is only a single peak at $E_x \sim 3$ MeV for KB3G. The summed $B(\mathrm{GT}_+)$ values are 6.20 and 5.37 for GXPF1J and KB3G, respectively (see Table II). The GT strength is more fragmented with non-negligible fraction of the strength in the high-energy region for GXPF1J as compared to KB3G.

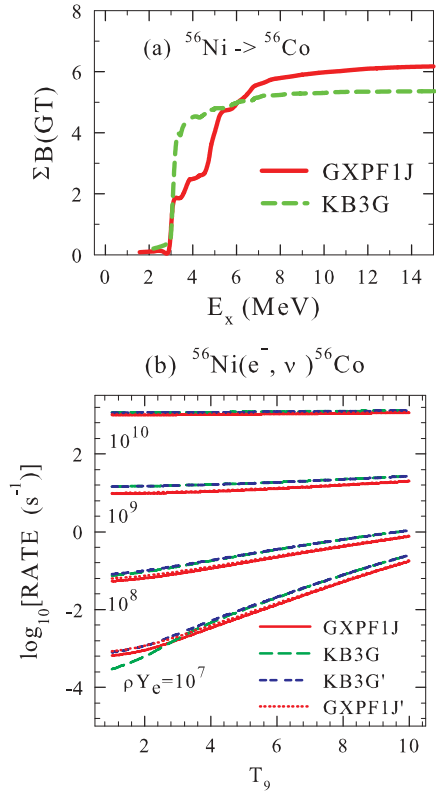

FIG. 5. (Color online) (a) Sum of the GT strengths for ^{56}Ni $\rightarrow$ ^{56}Co up to excitation energies of ^{56}Co, E_x, obtained for GXPF1J and KB3G. (b) Calculated electron capture rates on ^{56}Ni obtained by shell-model calculations with the use of GXPF1J (solid curves) and KB3G (dashed curves). The short-dashed (dotted) curves denoted as KB3G′ (GXPF1J′) are obtained by using the experimental excitation energy and B(GT) value for the transition to the first 1^+ state instead of the calculated values in the case of KB3G (GXPF1J).

This difference gives rise to a rather large difference in the capture rates as shown in Fig. 5(b). The capture rates for GXPF1J are reduced by ∼30% (10%) as compared to those for KB3G at $\rho Y_e = 10^7$–10^9 (10^{10}) g/cm^3, except for the case at $T_9 \leqslant 3$ for $\rho Y_e = 10^7$ g/cm^3. When the GT strength is shifted toward a higher-energy region, it becomes more difficult to induce the capture reactions, which results in the suppression of the capture rates. When the density is low and the electron chemical potential remains small, the GT strength in the low excitation energy region, particularly, the strength for the first 1^+ state at $E_x = 1.720$ MeV, is important.

The experimental value of the strength is available, $B(\mathrm{GT}_+) = 0.153$ [21]. We can use the experimental $B(\mathrm{GT}_+)$ value and the energy for the 1^+_1 state instead of the calculated ones: $B(GT_+) = 0.081$ (0.205) at $E_x = 1.570$ (2.196) MeV for GXPF1J (KB3G). The calculated results are shown in Fig. 5(b) and denoted as GXPF1J′ and KB3G′. The capture rates at $T_9 \leqslant 3$ for $\rho Y_e = 10^7$ g/cm^3 are considerably (slightly) enhanced in the case of KB3G (GXPF1J). This indicates that the energy position of the 1^+_1 state is important.

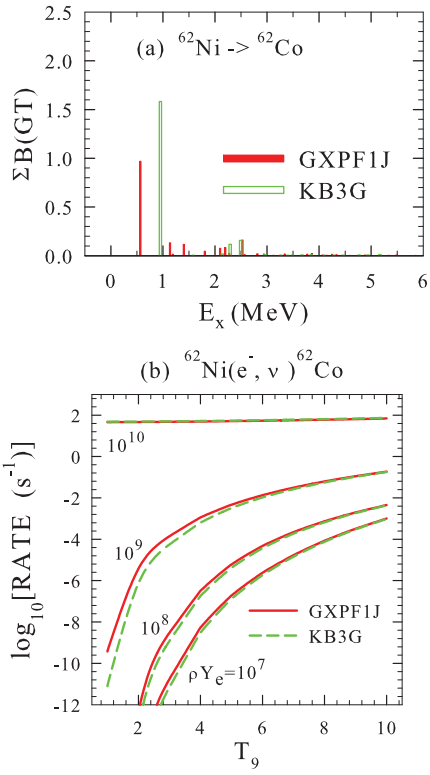

FIG. 6. (Color online) (a) GT strength for ^{62}Ni $\rightarrow$ ^{62}Co obtained by the shell-model calculation with the use of GXPF1J and KB3G. (b) Calculated electron capture rates on ^{62}Ni obtained by shell-model calculations with the use of GXPF1J (solid curves) and KB3G (dashed curves).

In other density and temperature regions, the effects on the rates are rather insignificant. The suppression of the capture rates for GXPF1J as compared to KB3G remains.

C. ^{62}Ni and ^{64}Ni

Finally, we discuss the capture rates on ^{62}Ni and ^{64}Ni. Neutron-rich isotopes also play important roles in the core-collapse processes. Calculated GT strengths in ^{62}Ni are shown in Fig. 6(a) for GXPF1J and KB3G. The first peak of the strength is located at a lower excitation energy region for GXPF1J than for KB3G while the total strength is smaller. The 1^+ states in ^{62}Co are observed at $E_x = 0.506$ and 0.530 MeV, which is consistent with the calculated energy position of the 1^+_1 state at $E_x = 0.568$ MeV obtained by GXPF1J. The calculated capture rates are shown in Fig. 6(b). We find that the rates for GXPF1J are larger than those for KB3G except for $\rho Y_e = 10^{10}$ g/cm^3. As the Q_{gg} value for the reaction is large and negative, $Q_{gg} = -5.826$ MeV, the calculated capture rates are affected mostly by the position of the first peak of the strength except for $\rho Y_e = 10^{10}$ g/cm^3.

Calculated GT strengths in ^{64}Ni are shown in Fig. 7(a) for GXPF1J and KB3G. The experimental GT strength for the ground state of ^{64}Co can be derived from the measured half-life of ^{64}Co and the branching ratio for the β-decay channel, ^{64}Co($1^+_{\rm g.s.}$) $\rightarrow$ ^{64}Ni($0^+_{\rm g.s.}$) [22]. The experimental strength is obtained to be $B(\mathrm{GT}_+) = 0.621$. This value is close to the calculated value of $B(\mathrm{GT}_+) = 0.706$ for GXPF1J, but smaller by $\sim$33% as compared to the calculated value for KB3G, $B(\mathrm{GT}_+) = 0.926$. The calculated capture rates are shown in Fig. 7(b). The rates are smaller for GXPF1J than for KB3G by a ratio of 0.76–0.77. This is very close to the ratio of the GT strengths of the two Hamiltonians at $E_x = 0.0$ MeV, $0.706/0.926 = 0.76$.

In both cases of ^{62}Ni and ^{64}Ni, calculated capture rates obtained by GXPF1J are very promising as the energy position of the GT strength in ^{62}Ni and the GT strength in ^{64}Ni obtained by GXPF1J are consistent with the observations.

IV. SUMMARY

In summary, we have studied electron capture reactions on ^{58}Ni and ^{60}Ni in stellar environments at high densities and high temperatures. Experimental GT_+ strengths are available for both of the isotopes. The observed GT_+ strengths as well as the capture rates obtained by experimental $B(\mathrm{GT}_+)$ values are found to be well reproduced, especially in ^{60}Ni, by shell-model calculations with the use of the GXPF1J Hamiltonian.

We have pointed out that the capture rates in ^{56}Ni differ by up to $\sim$30% between the GXPF1J and the KB3G Hamiltonians due to the large difference in the GT distributions. It would be quite interesting to obtain experimental information on the GT_+ strength in the unstable ^{56}Ni nucleus for excited 1^+ states in ^{56}Co.

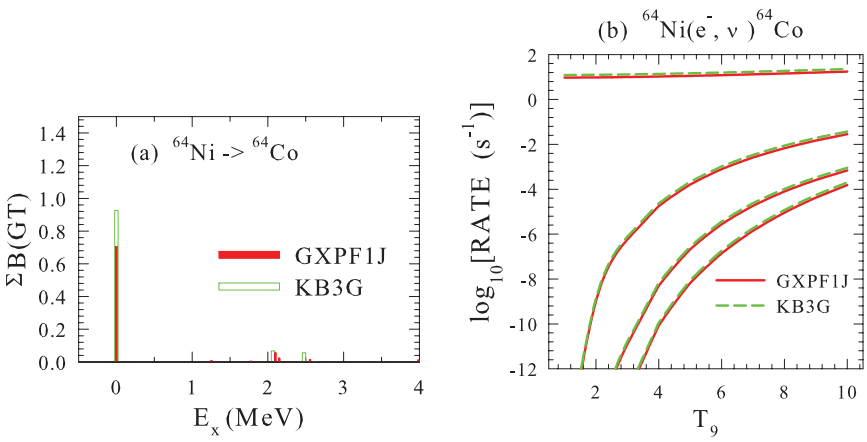

FIG. 7. (Color online) (a) The same as in Fig. 6(a) for ^{64}Ni $\rightarrow$ ^{64}Co. (b) The same as in Fig. 6(b) for ^{64}Ni.

We have also shown that the GXPF1J reproduces well the experimental energy position of the GT strength in ^{62}Ni, while in ^{64}Ni the experimental GT strength to the ground state of ^{64}Co is well reproduced by GXPF1J. This suggests the validity of the GXPF1J Hamiltonian in neutron-rich Ni isotopes.

The extension of the present work with the GXPF1J to other isotopes is under way. In odd-odd nuclei such as Co and Mn isotopes, the difference in the capture rates between the FFN and the shell-model calculations with the use of KB3 is significant [3]. The results of the investigation on Co and Mn as well as other isotopes will be reported in a forthcoming publication.

ACKNOWLEDGMENTS

The authors would like to thank K. Langanke and G. Martinez-Pinedo for useful communications on their work on capture reactions on Co isotopes. This work has been supported in part by Grants-in-Aid for Scientific Research (C) 22540290, (A) 20244035, and on Innovative Areas (20105004) of the Ministry of Education, Culture, Sports, Science and Technology of Japan, and also by JPSJ Core-to-Core Program, International Research Network for Exotic Femto Systems (EFES).

[1] G. M. Fuller, W. A. Fowler, and M. J. Newton, Astrophys. J. Suppl. Ser. **42**, 447 (1980); **48**, 279 (1982); Astrophys. J. **252**, 715 (1982); **293**, 1 (1985).
[2] K. Langanke and G. Martínez-Pinedo, Nucl. Phys. A **673**, 481 (2000).
[3] K. Langanke and G. Martínez-Pinedo, Phys. Lett. B **453**, 187 (1999).
[4] K. Langanke and G. Martínez-Pinedo, At. Data Nucl. Data Tables **79**, 1 (2001).
[5] E. Caurier, G. Martínez-Pinedo, F. Nowacki, A. Poves, and A. P. Zuker, Rev. Mod. Phys. **77**, 427 (2005).
[6] M. Hagemann *et al.*, Phys. Lett. B **579**, 251 (2004).
[7] A. Poves, J. Sánchez-Solano, E. Caurier, and F. Nowacki, Nucl. Phys. A **694**, 157 (2001).
[8] E. Caurier, K. Langanke, G. Martínez-Pinedo, and F. Nowacki, Nucl. Phys. A **653**, 439 (1999).
[9] N. Anantaraman *et al.*, Phys. Rev. C **78**, 065803 (2008).
[10] M. Honma, T. Otsuka, T. Mizusaki, M. Hjorth-Jensen, and B. A. Brown, J. Phys. Conf. Ser. **20**, 7 (2005).
[11] M. Honma, T. Otsuka, B. A. Brown, and T. Mizusaki, Phys. Rev. C **65**, 061301(R) (2002); **69**, 034335 (2004).
[12] M. Honma, T. Otsuka, B. A. Brown, and T. Mizusaki, Eur. Phys. J. A **25**, Suppl. 1, 499 (2005).
[13] W. Steffen, H.-D. Gräf, A. Richter, A. Härting, W. Weise, U. Deutschmann, G. Lahm, and R. Neuhausen, Nucl. Phys. A **404**, 413 (1983).
[14] P. von Neumann-Cosel, A. Poves, J. Retamosa, and A. Richter, Phys. Lett. B **443**, 1 (1998).
[15] G. Martínez-Pinedo, A. Poves, E. Caurier, and A. P. Zuker, Phys. Rev. C **53**, R2602 (1996).
[16] T. Mizusaki, RIKEN Accel. Prog. Rep. **33**, 14 (2000).
[17] R. R. Whitehead, in *Moment Methods in Many Fermion Systems*, edited by B. J. Dalton *et al.* (Plenum, New York, 1980), p. 235.
[18] T. Kajino, E. Shiino, H. Toki, B. A. Brown, and B. H. Wildenthal, Nucl. Phys. A **480**, 175 (1988).
[19] S. El-Kateb *et al.*, Phys. Rev. C **49**, 3128 (1994); A. L. Williams *et al.*, *ibid*. **51**, 1144 (1995).
[20] T. Suzuki, M. Honma, K. Higashiyama, T. Yoshida, T. Kajino, T. Otsuka, H. Umeda, and K. Nomoto, Phys. Rev. C **79**, 061603(R) (2009).
[21] H. Junde, Nucl. Data Sheets **86**, 315 (1999).
[22] B. Singh, Nucl. Data Sheets **108**, 197 (2007).